



university of
 groningen

faculty of science
 and engineering

kapteyn astronomical
 institute

BACHELOR RESEARCH PROJECT

Mining the Kilo-Degree Survey for Solar System objects

Exploring the classification of serendipitously observed asteroids

Ylse Anna de VRIES

s3197832

Supervised by:

dr. G. A. VERDOES KLEIJN

K. FRANTSEVA



October 11, 2019

Abstract

The main research assignment of this project was to characterise newly detected Solar System Object (SSO) candidates in the Kilo-Degree Survey (KiDS) which are found using an existing SSO detection pipeline. An additional harvest using the detection pipeline was performed on 31 single filter observation sets covering 29 different KiDS fields. This yielded 452 SSO candidates with an estimated false positive rate of 0.05%, adding to the 20221 candidates from an earlier 2018 harvest. Exploring how to further constrain the nature of the transient SSO detections by focusing on their heliocentric orbital distances, yielded two tentative approaches: a simplified method of population estimation for the SSOs, and a method of estimating the maximum admissible distance based on their motion. These approaches are currently implemented as python notebooks and can be used as extensions of the detection pipeline. Based on the analysis performed in this project there is no indication that the newly detected SSO candidates are systematically different from the already known population.

Acknowledgements

I would like to thank my supervisors Gijs Verdoes Kleijn and Katya Frantseva for their wonderful enthusiasm, support, and patience during the course of this project. The experience I gathered dipping my toes into the scientific process I will forever appreciate.

I would also like to thank Janke, Susan, Willeke and all the other inhabitants of the VIP room and Hydra cluster for their continuing emotional support and advice. As a sidenote: I both love and despise you for the distraction you provided.

I would also like to extend my thanks to the entire Kapteyn Astronomical Institute for providing such a safe and supportive environment.

Particular thanks to Jasper Postema for the use of some of his code which greatly helped with accessing the online services.

Special thanks to Janke Prins for the image of the VST telescope used in this thesis and the frontpage.

This research has made use of data and/or services provided by the International Astronomical Union's Minor Planet Center.

This project was presented with a poster at the annual conference for Astronomical Data Analysis and Software Systems (ADASS), a small version of the poster can be found in the appendices, or at: https://www.astro.rug.nl/~yadevries/BSc_Thesis/

Table of contents

	<i>Page</i>
1 Introduction	1
1.1 VLT Survey Telescope	1
1.2 The Kilo-Degree Survey	2
1.3 Astro-WISE	3
1.4 Minor planets	4
1.4.1 Nomenclature	4
1.4.2 Minor planet populations	5
1.4.3 Overview of minor planet populations	5
1.5 Coordinate systems	8
1.6 Research goals	9
1.6.1 The SSO pipeline	9
1.6.2 Population determination	10
2 Detecting SSOs in KiDS	12
2.1 Introduction	12
2.2 The SSO detection pipeline	12
2.2.1 Main concept and input	12
2.2.2 Source detection and apparent motions	13
2.2.3 Filtering proper SSO candidates	13
2.2.4 SkyBoT association	14
2.3 Results	15
3 Classifying the observed Solar System Objects	17
3.1 Introduction	17
3.2 Assuming circular orbits	17
3.2.1 Results	20
3.3 Admissable distances	23
3.3.1 Method	23
3.3.2 Results	24
4 Discussion	26
4.1 Serendipitous SSO detection	26
4.2 The circular orbit method	26

4.2.1	Population constraints	27
4.3	Maximum admissible distances	27
5	Conclusion	29
	Appendices	32
A	Constants for equation 3.8	33
B	ADASS poster	33

Introduction

In this Bachelor Research Project our main aim was to detect Solar System objects in the Kilo-Degree Survey (KiDS) (Kuijken et al. 2019) using an existing detection pipeline. Furthermore, we wanted to explore methods of categorising these highly transient detections of minor planets. The following chapter will hopefully provide the reader with the necessary background to understand our methodology and reasoning.

The KiDS data used in this project has been collected with the VLT Survey Telescope (VST) and subsequently stored and processed within the Astro-WISE environment. In the following sections of this introduction I will briefly introduce each of these topics, as they form the foundation of this project.

Tying into the further analysis we want to perform on these Solar System objects, I will give a brief overview of minor planet populations in general and the minor planet populations found in Solar System, together with a brief reference chapter on the coordinate systems used throughout the project.

In the final section I will further describe and motivate the research goals we set out to cover with this project.

1.1 · VLT Survey Telescope



Figure 1.1: The VLT Survey Telescope at ESO's Paranal Observatory in May 2019.

IMAGE CREDIT: Janke Prins

The VST was commissioned in 2011 at the ESO Paranal observatory in Chile (Capaccioli and Schipani 2011). It was designed with a scientific focus on wide-field surveys, to study, for instance, extragalactic sources and gravitational lensing (Capaccioli, Mancini, and Sedmak 2003).

The VST uses a two mirror Ritchey-Chrétien setup, with a 2.61 m aperture. It also includes active optics and various lenses and compensators for the correction of atmospheric and wide-field aberrations (Capaccioli and Schipani 2011).

The VST uses a single instrument, an optical wide-field camera called OmegaCAM, developed by a consortium including groups from the Netherlands, Germany and Italy. The OmegaCAM uses a 32 CCD grid, with each CCD having 2000x4000 pixels. It images one full square degree of the sky at 0.21 arcsecond resolution (Kuijken 2011).

The OmegaCAM has 12 filters available, the Sloan u, g, r, i, z filters and the B and V filters, the medium-passband Strömgren- v filter and various narrow band filters. They are robotically placed in front of the detectors (Kuijken 2011).

1.2 · The Kilo-Degree Survey

The Kilo-Degree Survey (KiDS) is a wide-field optical imaging survey that uses the ESO VST telescope (Kuijken et al. 2019). The main scientific focus of the survey is to study weak gravitational lensing and redshifts to constrain the cosmological matter distribution (J. T. A. de Jong et al. 2013). The survey is divided between two fields on the southern sky, see Figure 1.3 (Kuijken et al. 2019).

As described in Jelte T. A. de Jong et al. 2015, the survey is conducted in the optical u, g, r and i filter bands. The individual fields are each observed to a high depth in any given filter in a single epoch, as opposed to observing each filter shortly and returning to the same filter and field later multiple times.* This ensures that when data is released intermediately, it is at the designed depth for the survey and can already be used for some of the science goals of the survey.

However, as this pattern is also designed to only observe in a given filter and a given field when appropriate observational conditions are reached, the survey observes in a patchy manner across the sky. This means that the time between observations of the same field in different filters can vary from days to years. Naturally, this fits the goal of observing relatively invariant extra-galactic objects, but makes the survey generally limited when it comes to more sources more variable than these timescales.*

* Additionally, a second pass of the i -band is on-going near the end of the survey, mostly to improve image quality (Kuijken et al. 2019)

* The i -band re-pass also only allows variability studies on timescales of multiple years (Kuijken et al. 2019)

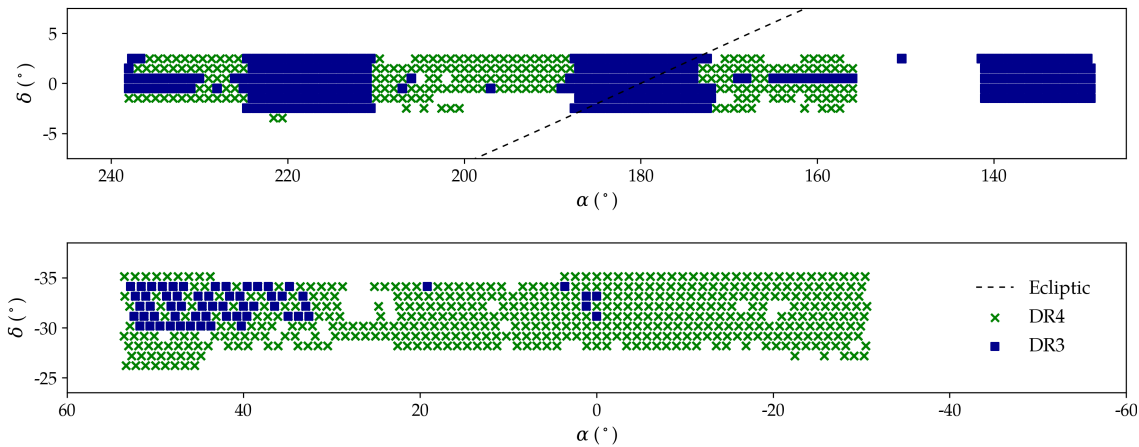


Figure 1.2: An overview of the locations on the celestial plane of the KiDS tiles, distinguishing between the third and fourth data releases (squares and crosses respectively) on both the KiDS North (top) and South (bottom) fields. The Solar System ecliptic is also shown (Kuijken et al. 2019).

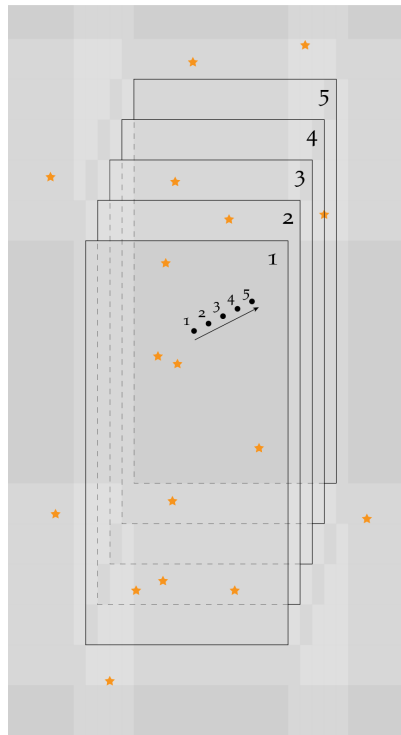


Figure 1.3: A schematic overview of the dithering strategy employed in KiDS observations. Note that in subsequent frames an SSO (black dot) would move, while objects with considerably lower to no proper motion – like stars and galaxies (yellow stars) – do not seem to move. Each of the dithered frames is offset on the celestial plane, the background does not move (Kuijken et al. 2019, **Also follows:** <http://kids.strw.leidenuniv.nl/>, Accessed on 07/05/2019)

Due to the design of the OmegaCAM focal plane, any single exposure consists out of 32 individual CCD images, with some small gaps in between. As is illustrated in Figure 1.2, to fill these gaps any observation of a filter consists out of five (for the g , r and i bands) or four (for the u band) exposures that are ‘dithered’, or offset slightly by a number of arcseconds to get a complete observation of a given field in a filter (Jelte T. A. de Jong et al. 2015). The dithering strategy lies at the core of SSO observations in KiDS, more in section 2.2.

1.3 · Astro-WISE

All data of VST surveys is stored on the Astronomical Wide-field Imaging System for Europe (Astro-WISE), Astro-WISE is an information system that uses an international network of storage servers, computing clusters, and databases to store and process the data from large scale surveys (Valentijn et al. 2007). Astro-WISE was initially set up to enable researchers from across the world to access and process data from the VST telescope. The scale of the expected data sets from the VST’s OmegaCAM instrument meant that Astro-WISE had to be designed to handle petabytes of data and have a computing speed in the teraflop* range (Begeman et al. 2013).

As is described in much greater detail in Valentijn et al. 2007, Astro-WISE uses a dynamic approach to data distribution and processing. It performs and logs every

* 10^{12} floating point operations per second

step of the data reduction procedure, and even the relevant data for the instruments in a comprehensive system. This means that any user can jump in or out at any place of the regular data reduction pipeline, for their specific goals.

For instance, one user could produce lists of astrophysical sources in a given field through the dedicated processing units within Astro-WISE, with appropriate logs and with these source lists being stored immediately, such that later another user could confidently use the same source lists by only accessing Astro-WISE. However, at any other time yet another user that wishes to use completely raw data to test a certain technique can get the raw frames through Astro-WISE as well.

1.4 · Minor planets

Now we go from the subjects necessary for data collection and processing to a subject about categorising the Solar System objects (SSOs) we have detected. The detection pipeline will be described in section 2.2 of the Methods chapter.

1.4.1 — Nomenclature

Firstly it is convenient to know which terminology is used. Within this project – and in general – the terms *Solar System object*, *minor planet* and *asteroid* are used somewhat interchangeably, although all three are distinct.

Solar System objects are any object found within the Solar System. They are a category inclusive of, but distinct from, minor planets as they can also, for instance, include man-made objects or interstellar visitors. It is the most broad and therefore generally correct way to refer to any unknown detection within the Solar System.

Minor planets are all objects, excluding the eight major planets, that orbit the Sun. They range from tiny dust particles to dwarf planets. **Asteroids** are rocky minor planets that orbit interior to or are co-orbital with Jupiter. Asteroids are kept distinct from other rocky minor planets as those found beyond the orbit of Jupiter often have different (icy) surface features (Pater and Lissauer 2001).

Within this project the vast majority of objects we can classify are asteroids (Mahlke, Bouy, et al. 2018) and in our later analysis you will also find we can only really study asteroids to a significant extent. I hope this somewhat justifies the occasional mixing of terms, but the reader should keep the proper terminology in mind.

Additionally, it can also be important to know when a minor planet is considered to be a **discovery** and receives a **designation**. At the Minor Planet Center (MPC) minor planets are only considered to have been discovered if they were observed roughly three times in two separate nights (Spahr 2010). They then receive a preliminary designation, which consists of the year of discovery and a sequence of letters and numbers indicating a more exact time and order of discovery, e.g. 2003 UB₃₁₃ (Pater and Lissauer 2001).

When this minor planet is then subsequently observed enough to get a good orbit determination, it will be officially numbered and eventually receive a **name**, e.g. 1 Ceres or 532 Herculina (Pater and Lissauer 2001).

1.4.2 — Minor planet populations

Minor planet populations describe the orbital distribution of minor planets. So the classification is based on orbital elements like the semi-major axis – which can also be understood as the mean distance to the Sun – and the perihelion or periodicity of the asteroids. Minor planet populations in principle say nothing about the composition or size of the minor planets, although this is of course often studied on a population basis (Pater and Lissauer 2001).

The importance of population statistics cannot be understated. The different populations are all interrelated. A minor planet (or minor planet fragment) may be scattered into another population by gravitational perturbations or thermal effects (Jedicke et al. 2015). Such is, for instance, the origin of the current asteroids in the Near Earth population. Asteroids which can also be potentially hazardous to Earth (Pater and Lissauer 2001). Knowing one population's properties can help constrain the properties of other populations.

Additionally, the minor planets were assumedly all, just like the major planets, formed in the earliest stages of the Solar System. Therefore they are of importance to our understanding of its formation. The distributions can inform our models of the early Solar System. They for instance suggest that many Main Belt asteroids were formed elsewhere in the early Solar System and migrated to their current orbit (Jedicke et al. 2015). Knowing the number, orbital elements and other properties of Main Belt asteroids could therefore inform these models.

There are of course more factors to study with respect to populations and minor planets, all using various observational methods. Using only optical data the number of factors to study is limited, although it can be very robust when used together with other observations. Such as how thermal and optical emissions of minor planets can be combined to calculate their size and albedo (Pater and Lissauer 2001).

1.4.3 — Overview of minor planet populations

*Most of the population descriptions I will give follow those given in the book Planetary Sciences (Pater and Lissauer 2001), however for the exact semi-major axis and perihelion ranges I use those given by the documentation of the SkyBoT tool.**

In the following section I will provide brief descriptions and definitions of various populations we currently identify, as a quick reference. The following list is not exhaustive, but it should give an overview of all the populations that are relevant to this project. See also Figure 1.4, for a schematic overview of the distribution of the minor planet populations.

* **Found at:**
[vo.imcce.fr/
webservices/
skybot/
?documentation](http://vo.imcce.fr/webservices/skybot/?documentation)

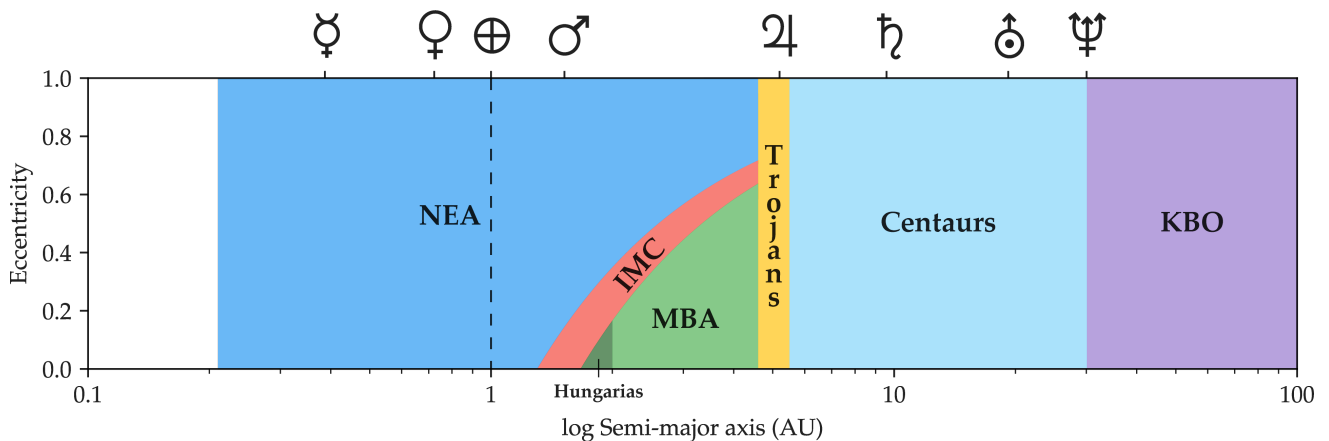


Figure 1.4: A schematic overview of the distribution of minor planet populations in the Solar System, categorised by the semi-major axis and eccentricity ranges, the semi-major axes of the major planets are also shown. Shown are the populations we distinguish in this project. Listed from inner to outer populations: Near Earth Asteroids (NEA, blue), Intermediate Mars Crossers (IMC, red), Hungarias (dark green), Main Belt Asteroids (MBA, green), Trojans (yellow), Centaurs (light blue) and Kuiper Belt objects (KBO, purple). Note the relationship between the perihelion distance (r), semi-major axis (a) and eccentricity (e): $r = a(1 - e)$, which explains how high a and e NEAs still have perihelia below 1.3 AU. **Definitions and figure based on:** vo.imcce.fr/webservices/skybot/?documentation.

Near Earth Asteroids

The near Earth asteroids (NEAs) are asteroids which have orbits that come close to Earth's orbit. They have semi-major axes between 0.21 and 2.0 AU and perihelia below 1.3 AU.

The NEAs have quite chaotic and unstable orbits, their dynamical lifetime is short at less than 10^7 years. To maintain the existence of the population it is suggested, and generally accepted, that the NEA population is constantly replenished from the edges of the orbits of more stable populations – for instance Main Belt Asteroids near any of the Kirkwood gaps.

Intermediate Mars-crossers

Intermediate Mars-Crossers (IMCs) are asteroids in orbits that cross the orbit of Mars, but do not come close to Earth, although sometimes they are classified as NEAs as well. They have semi-major axes between 1.0 and 2.0 AU, and perihelia between 1.3 and 1.66 AU. They have similarly chaotic orbits to NEAs, and therefore also have to be replenished from more stable populations.

Hungarias

The Hungaria asteroids, named for their biggest member 434 Hungaria, is the innermost dense group of asteroids (Spratt 1990). They have semi-major axes between 1.0 and 2.0 AU and perihelia above 1.666 AU. Sometimes they are counted as the innermost family of Main Belt asteroids, although they have a unique relationship with Mars compared to the other Main Belt groups (Spratt 1990). Therefore we treat them separately within this project.

The gap caused by the 4:1 mean motion resonance with Jupiter forms the outermost boundary of the group, while their innermost boundary is posed to be caused by the constant influence of Mars. They also have uniquely high inclinations, between 16 and 33° and very low eccentricities at around 0.18. The low eccentricity is probably a result of Mars 'pushing' the group towards the outer boundary (Spratt 1990) and similarly the high inclination causes the asteroids to often be further away from the ecliptic, again avoiding the influence of Mars (Milani, Knežević, et al. 2010). The Hungaria region is therefore also thought to have been bigger in the past (Spratt 1990).

Main belt asteroids

The population of Main Belt Asteroids (MBAs) is by far the most well-known, it is also significantly larger than any of the populations with perihelia closer to the Sun. The Main Asteroid Belt contains asteroids with semi-major axes between 2.0 and 4.6 AU, although often the Hungarias are also included, which broadens this range. Additionally one should keep in mind that many NEAs also cross the orbits of the Main Belt, but have significantly lower perihelia.

Within the MBAs various subpopulations are distinguished mainly based on their orbital period. This is due to a number of gaps that can be observed when one looks at the orbital periods of the asteroids. These gaps are called Kirkwood gaps after Daniel Kirkwood who discovered them in 1867. The gaps are caused by mean motion resonances with the orbit of – mainly – Jupiter, such as the resonance gap between the Hungarias and inner MBAs.

Trojans

Trojans are asteroids found at the L_4 and L_5 Sun-Jupiter Lagrangian points. Therefore they have semi-major axes between 4.6 and 5.5 AU, at roughly the same orbital distance as Jupiter. Jupiter seems to be the only planet shepherding such a significant population at its stable triangular Lagrangian points.

Centaur

The Centaurs are a dynamically unstable population of minor planets between the orbits of Jupiter and Neptune, with semi-major axes between 5.5 and 30.1 AU. They have highly chaotic orbits and dynamical lifetimes of roughly 10^6 to 10^8 years. Some are speculated to be dormant comets, and most probably originate from the more distant Kuiper Belt.

Kuiper Belt Objects

Kuiper Belt Objects (KBOs), also sometimes or interchangeably called Trans Neptunian Objects (TNOs), are objects found in the Kuiper Belt beyond the orbit of Neptune. Their orbits have semi-major axes between 30.1 and 2000.0 AU, beyond which the Kuiper Belt transitions into the Inner Oort Cloud.

Many of the KBOs, called classical KBOs (CKBOs), have very low eccentricity orbits with relatively stable mean motion resonances with Neptune. The minor planet 134340 Pluto is probably the most well known CKBO, at a mean motion resonance of 3:2 with Neptune.

Scattered Disk Objects, another subpopulation of KBOs (or a subset of TNOs next to KBOs, depending on which definitions are used), have non-resonant, highly eccentric orbits and are thought to be scattered either from the inner populations or from the Oort Cloud.

1.5 · Coordinate systems

All of the general concepts and equations in the following section are based on the book *Fundamental Astronomy* (Karttunen et al. 1987).

Within this research project we are looking at minor planets; objects for which it is convenient to look in a frame of reference based on the Solar System. However, generally celestial coordinates in astronomy are given in the equatorial system. This system is based on Earth's rotational axis, which is somewhat decoupled from the Solar System due to its tilt. In this section I will describe both the equatorial system and the ecliptic system, of which the latter solves this issue.

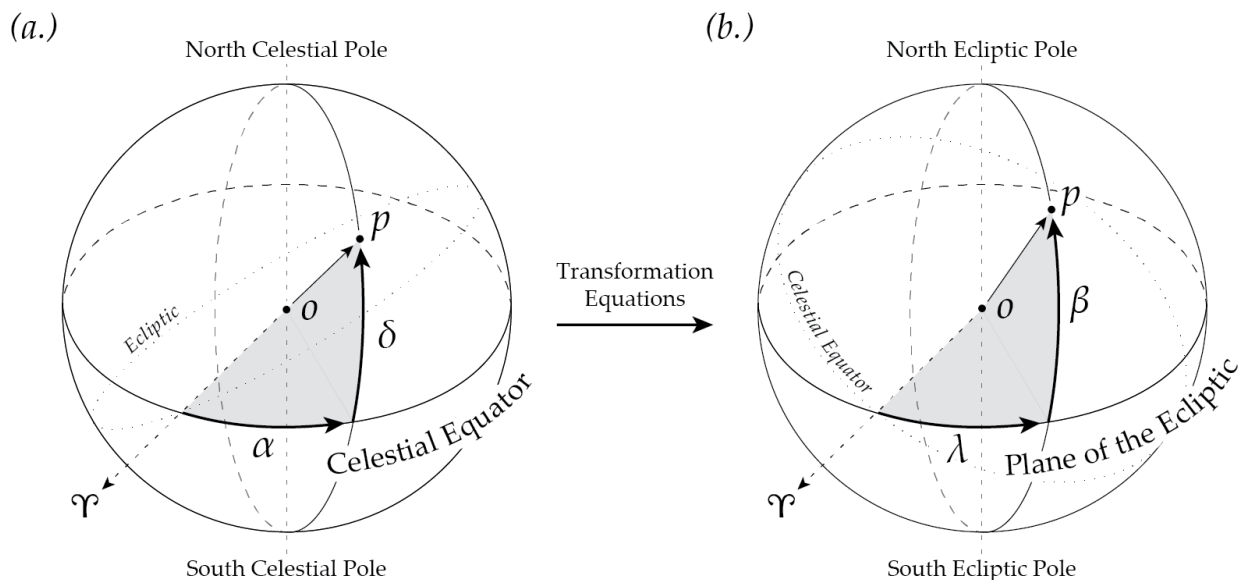


Figure 1.5: A schematic overview of both the equatorial (a.) and ecliptic (b.) coordinate systems. The relative positions of the the equatorial and ecliptic planes and their respective poles are indicated. The equatorial and ecliptic coordinate systems indicate the position (p) of an object through either their right ascension (α) and declination (δ), or their longitude (λ) and latitude (β), respectively. The origin (o) of both systems is arbitrary, but is generally chosen to be either the Earth or the Sun. Both use the vernal equinox (γ) as their principal reference axis.

In the equatorial system, the reference plane – that is the great circle describing zero declination – is a projection of the Earth equator unto the celestial plane and the principal axis is pointing towards the vernal equinox. Declination (δ) describes the angular separation from the celestial equator and right ascension (α) describes the angular separation from the vernal equinox along the equator, see Figure 1.5a. Due to

the precession of the Earth's rotational axis, the celestial equator and its poles shift slightly over the course of thousands of years. Therefore the coordinate system has to be fixed to a certain epoch.

For describing positions in Solar System another coordinate system based on the ecliptic is more convenient. The ecliptic is the plane formed by the orbit of the Earth around the Sun or by the movement of the Sun across the sky, from Earth's perspective. Most major and minor bodies of the Solar System orbit roughly within this plane. In the ecliptic coordinate system, coordinates are described in latitude (λ) and longitude (β) (equivalent to the right ascension and declination, respectively), the reference axis is still based on the vernal equinox, see Figure 1.5b.

Both systems's origins can vary, although most common are either the Earth or Sun. Using the origin, when an object has a fully determined position, one can add a third coordinate in the form of the distance.

1.6 · Research goals

1.6.1 — The SSO pipeline

During an internship at ESA (then) master student Max Mahlke started developing a pipeline for the detection of SSOs in wide-field surveys. The pipeline was finished as a master's thesis at the University of Aachen and a follow-up paper published: Mahlke, Bouy, et al. 2018. As is explained there, tapping into this previously unused and unlikely source of SSO detections can help determine orbits for minor bodies. Orbits which in turn can help constrain models for the Solar System's formation history and their current influence on other Solar System bodies.*

Using this pipeline, as part of the original research at the University of Aachen, an SSO search was performed on 346 square degrees from the third data release of KiDS (DR3), which is around 65% of that data set. This yielded 20221 SSO candidates with an estimated 0.05% false positive rate. More of the data release was not studied due to time constraints.

In March 2019 the fourth data release of KiDS (DR4) was presented, with 1006 deg² of the sky surveyed in the *ugri* bands (Kuijken et al. 2019). The primary science goal of this bachelor research project is to extend the SSO search in KiDS using the existing pipeline with this new DR4 data. As the pipeline forms an integral part of this research project, the pipeline is described in more detail in section 2.2 of the Methods chapter.

In the July 2019 issue of *Astronomy and Computing*, M. Mahlke presented a generalised and further developed version of SSO pipeline, called *SSOS*. The SSO pipeline up to that point was still specifically tailored to KiDS, as a proof-of-concept. *SSOS* should offer the capabilities of the KiDS SSO pipeline for any suitable survey, opening up significantly more SSO detections (Mahlke, Solano, et al. 2019). The 2019 version of the SSO pipeline is no longer directly suitable for KiDS, thus in this project the 2018 version is used as a time saving measure.

* See the previous section 1.4 for more on asteroid populations and their significance.

1.6.2 — Population determination

Beside observing the SSOs in KiDS using the pipeline, we would also like to perform some further analysis on the observed SSOs. Especially on those SSOs that have been observed but cannot be associated with any known asteroids.

Within the initial set of SSO observations from 2017, only 53.4% of the asteroids were associated. The remaining 46.6% of the SSO harvest could still host a lot of information, especially as KiDS has a significantly higher depth – it effectively observes to a higher magnitude – compared to more conventional SSO searches (Mahlke, Bouy, et al. 2018), see Figure 1.6 for an illustrative plot.

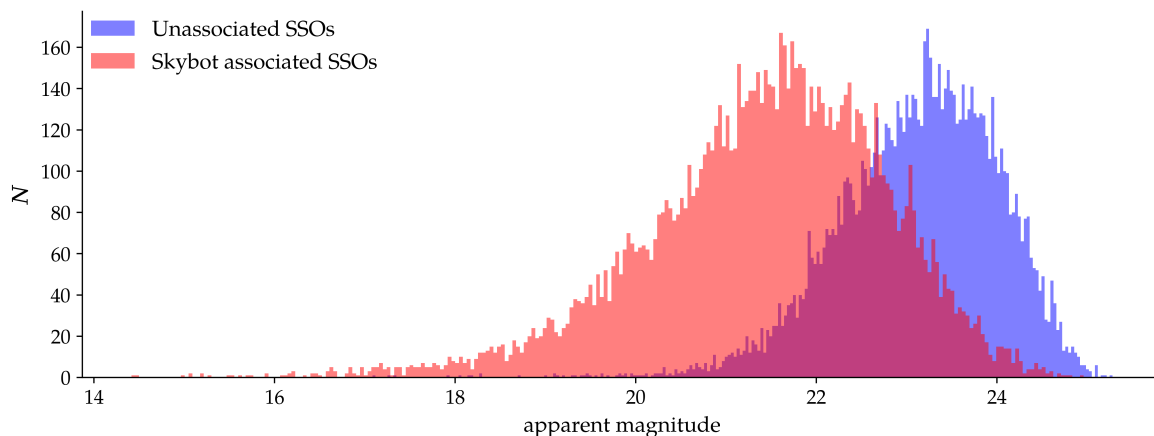


Figure 1.6: The above histogram shows the distributions of observed apparent magnitudes for SSOs detected in KiDS, during an SSO search in 2018 (Mahlke, Bouy, et al. 2018), between the SkyBOT associated – known – SSOs (red) and the unassociated SSOs (blue). SkyBoT is explained in section 2.2.

The high depth coupled with the lack of association suggest that these SSOs have not previously been detected (Mahlke, Bouy, et al. 2018), and are thus highly intriguing. However, these unassociated SSOs are transient detections in a survey which is not tailored for SSO detections, often called serendipitous detections. They very often lack the necessary timespan in their observations and it not possible to perform conventional methods for orbital or distance determination. These determinations are of course often the first step before any further analysis.

In Milani, Gronchi, et al. 2004 this concept is explored. They explain how orbital determination methods like Gauss’s method, first developed to re-observe the first minor planet discovered, 1 Ceres (Gronchi 2005), break down because the observed ‘arcs’ traced by serendipitous detections, have no or too small curvature. A low curvature in turn leads to a very high uncertainty in the orbital determination. They call these Too Short Arcs (TSAs), and subsequently perform a very impressive analysis to determine statistical admissible ranges for these asteroids’ orbits (Milani, Gronchi, et al. 2004).

This analysis is incredibly rigorous and in level significantly beyond the scope of this project. This makes it unfeasible to perform this kind of analysis on our kind

of samples. Especially as there is of the order 10^4 serendipitous SSO candidates to be found in KiDS. However, with our prior knowledge of minor planet populations, we hypothesise that it is possible to get significant population estimations for serendipitous SSOs using relatively simple assumptions about the majority of these SSOs.

Therefore, a secondary research goal of this project is to explore computationally simple methods of minor planet population determination to hopefully gain – even a little – more information about the unassociated SSOs found in KiDS.

Detecting SSOs in KiDS

2.1 · Introduction

The data processing pipeline used in this project to find SSOs was developed from 2016 to 2018 by Max Mahlke as part of his ESA internship project. In the following section I will detail the general methodology of this SSO detection pipeline.

In section 2.3 I will show the results of this pipeline when performed on KiDS data. These results include both the SSO search performed by M. Mahlke for his paper, Mahlke, Bouy, et al. 2018, on DR3 data, and a smaller search performed for this project, including some of the DR4 data.

Chapter 3 will detail some of the analyses that we explored to categorise the results gathered from the SSO pipeline.

2.2 · The SSO detection pipeline

Throughout this section I will use information from Mahlke, Bouy, et al. 2018.

In this section I will go through the main conceptual steps of the SSO pipeline. However, for any of the exact parameters and methodology to reproduce the pipeline I would refer any reader to Mahlke, Bouy, et al. 2018, or to Mahlke, Solano, et al. 2019, which details a generalised and further developed version of the same pipeline used in this project.

2.2.1 — Main concept and input

The pipeline is based on the simple fact that, generally, nearby Solar System objects exhibit much larger apparent motions across the sky than any sources outside the Solar System. So to detect SSOs we have to detect significant apparent motion.

As is explained in Section 1.2, the KiDS observation strategy is generally badly suited for detecting celestial movement or magnitude changes. KiDS focuses on extra-galactic sources which tend to barely move on the sky over the course of years. As is explained in the same section and Figure 1.2, however, KiDS does employ dithering to account for CCD gaps in the OmegaCAM instrument. The time between the different exposures performed as part of this dithering strategy allows us to study variability over a range of roughly 20 minutes, which is enough for the apparent motions exhibited by SSOs (upwards of a few arcseconds per hour).

We have to study the separate exposures of any observation in a given filter and field. Thus, as the first step, the pipeline queries so-called REGRIDDEDSCIENCEFRAMES from the Astro-WISE system for any selected field and filter. These frames have been astrometrically and photometrically calibrated, and have been provided with pixel value statistical weight maps by the Astro-WISE data pipeline. These weight maps are taken into account by the SSO pipeline, and can account for telescope inherent irregularities like dead pixels.

These frames account for all the images made by each CCD in the focal plane. The

focal plane of the OmegaCAM instrument consists out of 32 CCDs, 1000x2000 pixels each. For each filter-field combination there are a number of exposures as part of the dithering strategy, five for the g , r and i filters, four for the u filter. Meaning that, in total, any processing of a filter-field combination has to go through either $(5 \times 32 =) 160$ or 128 individual REGRIDDEDSCIENCEFRAMES.

2.2.2 — Source detection and apparent motions

When the frames have been obtained by the pipeline, we want to track and categorise the astronomical objects contained within them, so we can filter out the fast moving SSOs. Computationally you cannot simply compare pixel based images, so the detectable sources have to first be separated and placed at the proper coordinates for each frame, before we can compare their motions.

In the SSO pipeline the common program SExtractor (short for Source Extractor, Bertin and Arnouts 1996) is employed to find the sources in the individual frames. This subtracts the background, finds the sources and performs further advanced analyses. For the SSO pipeline the parameters are set in a manner favourable for finding small simple point sources, like the SSOs we wish to detect. SExtractor outputs source lists of all the sources found in each frame.

Subsequently the program SCAMP (Bertin 2006) analyses these SExtractor source lists frame by frame sequentially over the five or four exposures. It also compares the sources found with catalogues of known sources to more accurately calibrate the positions. Moving objects are cross-matched up to a radius that allows for apparent motions of up to $200''/h$. The apparent motions are subsequently calculated using a linear least squares fit across all the cross-matched sources. SCAMP also finds the visual magnitude for each source.

Now the SSO pipeline has a list of assumedly moving sources in the field-filter combination, that form our SSO candidates. Of these candidates we know their positions, calculated apparent motions, parameters describing their shape, and visual magnitude. It is however unsure how many of these moving sources actually fulfil the requirements to be SSOs.

2.2.3 — Filtering proper SSO candidates

A number of steps are taken to filter out the non-SSO contaminants from our sample of moving SSO candidates. Firstly it is important to know the main contaminants that were found to be present.

Cosmic ray detections sometimes occur twice within the cross-match radius set by SCAMP, therefore appearing as moving objects. **Diffraction patterns and bright star halos** can also seem to move across multiple exposures and bright parts of them can be seen as separate (moving) sources. When it comes to the detection of slow moving minor planets, like KBOs, **stars and galaxies** can become contaminants as their apparent motions can be similar to some SSOs.

The first step that was found to be very effective to take out contaminants was to set a lower limit on the number of cross-matched detections needed to call a source an SSO. This is done by requiring four or more detections within the exposures of a single

filter-field combination. This very effectively filters out cosmic ray detections, but also excludes those SSOs with only two or three subsequent detections, in Mahlke, Bouy, et al. 2018 the effect of lowering the number of detections needed is discussed.

The next big step is requiring linearity of the proper motions, many of the cosmic ray detections, parts of bright star halos and diffraction patterns, and stars and galaxies exhibit (very) non-linear motion. Meanwhile, the motion of the SSOs within the short dithering time span is essentially linear.* By requiring the R^2 parameter of a linear least squares fit of the motion to be above 95%, these non-linear motions are greatly filtered out.

Similarly, constraints are put on the magnitude and relative error of the measured apparent motions, based on the intrinsic limits of the survey. Sources that move slower or faster than should be observable or whose motions are hard to be determined can be disregarded as they are increasingly likely to be contaminants.

The following filtering steps use the shape parameters determined by SExtractor. Firstly by looking for any variability in the shape of an SSO candidate over the four or five observations. Point-source-like objects, like SSOs, that are moving in one direction, and that are observed for an equal time during each exposure, should exhibit the same shape during each observation. Highly variably shaped objects can therefore be excluded. Similarly, highly extended sources (larger than 95% of the rest of the sources in the same exposure) were found to likely be misidentified bright star halos and diffraction patterns.

As a final step all candidates within 200 arcseconds of known bright sources from the HYG catalog are excluded, as it was found that of a given sample most of the artefacts that remained were close to the bright stars.

With the final filtering step the main detection pipeline has concluded. In Mahlke, Bouy, et al. 2018 the results and possible errors and improvements are discussed in detail, I do wish to highlight that the entire pipeline was set up for a pure, rather than complete, sample and the completeness has not been rigorously tested.

2.2.4 — SkyBoT association

As a final step to the pipeline, the SkyBoT utility (Berthier et al. 2006) provided by the IMCCE is used to find as many asteroids that have previously been assigned designations. The SkyBoT utility consists out of a database of pre-computed ephemerides of all designated minor planets, and allows for any user to provide coordinates for observed SSOs and search for any known asteroids within a certain radius around their own observations. The designations of the associated asteroids are added to the output of the pipeline.

This final step is useful for comparative study as we can now know most relevant orbital elements of the associated minor planets that were observed. This will be important for our later analysis.

* This ties directly into the fact that these SSO detections exhibit Too Short Arcs, as discussed in section 1.6.2.

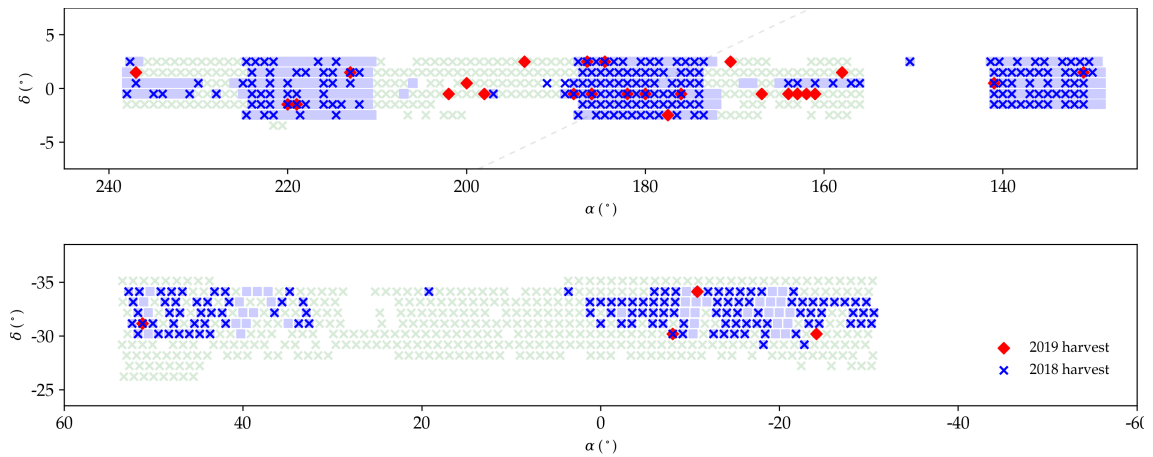


Figure 2.1: An overview of the KiDS tiles on the celestial plane for which one or more filters were used in an SSO search, both the earlier harvest by M. Mahlke (Mahlke, Bouy, et al. 2018) and the search performed for this project. The plot is overlaid on Figure 1.3 from section 1.2.

2.3 · Results

For this project the SSO pipeline was performed on 29 fields for a total of 31 filter bands. Combined with the SSO search performed by M. Mahlke (Mahlke, Bouy, et al. 2018) 362 square degrees of the celestial plane were searched for SSOs in at least one filter band. All fields are shown in Figure 2.1. In accordance with Mahlke, Bouy, et al. 2018, both searches have an estimated 0.05% false-positive rate, for the filter settings used. A full discussion on the purity of the sample can be found in Mahlke, Bouy, et al. 2018.

The search performed for this project yielded 452 SSO candidates, together with the 20221 candidates from the Mahlke search, this means a total of 20673 SSO candidates have been found in KiDS thus far. During both searches the SkyBoT service was used to associated the SSOs with known minor planets. Of our search 249 SSOs were associated, with 10754 associated SSOs in the 2018 search. The locations of the SSO detections are shown in an overview plot in Figure 2.2, distinguishing between SkyBoT associated and unassociated SSOs. Interestingly, it can be seen here that the associated SSOs are mostly concentrated around the ecliptic, this shows how SSO searches – and minor planets in general – are concentrated around the Solar System ecliptic, as can be expected.

Using the IMCCE Solar system Open Database Network (SsODNet) the accompanying minor planets population were found for most of the associated SSOs. In Table 2.1 the distribution of the associated SSOs over their minor planets populations is listed, for both our and the earlier SSO harvest.

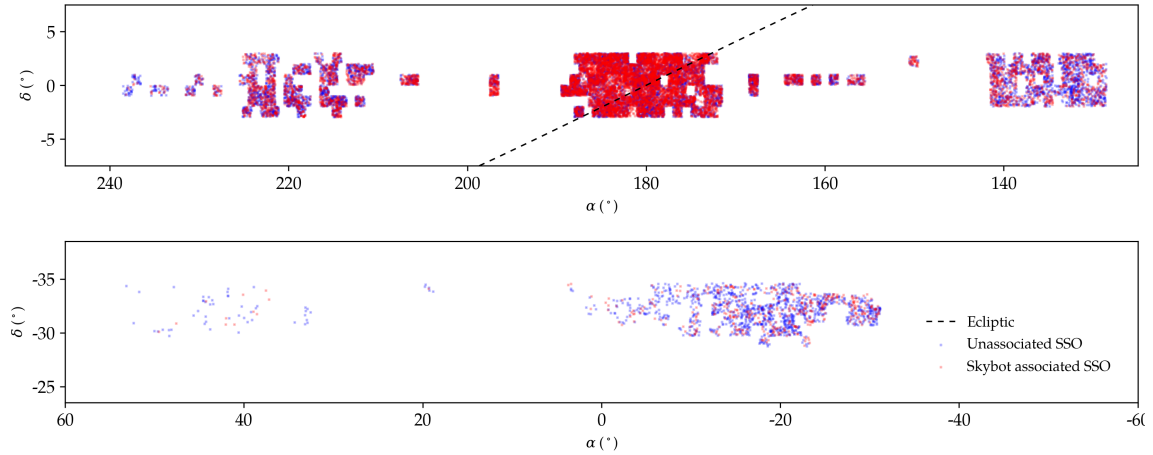


Figure 2.2: An overview of the locations on the celestial plane where SSOs were found, distinguishing between SkyBoT (Berthier et al. 2006) associated and unassociated SSOs. Note that there are less associated minor planets outside the ecliptic. Both the earlier harvest by M. Mahlke (Mahlke, Bouy, et al. 2018) and the search performed for this project are included.

		NEAs	IMC	Hungaria	MBA	Trojans	Centaur	KBOs	Undet.	Total
2019 harvest	number	0	6	0	535	10	0	1	0	552
	percentage	0.0%	1.09%	0.0%	96.92%	1.81%	0.0%	0.18%	0.0%	
Mahlke harvest	number	12	79	50	10400	147	1	4	61	10754
	percentage	0.11%	0.73%	0.46%	96.71%	1.37%	0.01%	0.04%	0.57%	
Total	number	12	85	50	10935	157	1	5	61	11306
	percentage	0.11 %	0.75 %	0.44 %	96.72 %	1.39 %	0.01 %	0.04 %	0.54 %	

Table 2.1: Distribution of minor planets associated by SkyBoT over the minor planet populations as found by the IMCCE SsoODNet web service. Both the earlier harvest by M. Mahlke (Mahlke, Bouy, et al. 2018) and the search performed for this project are included. See section 1.4 for the abbreviations, the label 'Undet.' means that no population classification could be found in the database.

Classifying the observed Solar System Objects

3.1 · Introduction

Any subsequent analysis of the SSOs that were retrieved using the SSO pipeline has to keep in mind the inherent limitations of the observations strategy. Limitations that are generally inherent to serendipitous SSO detections. The limitations were also treated in section 1.6.2.

We do not know the distance with respect to the observer, which means we cannot precisely infer any absolute magnitude and therefore size. We also do not know the radial motion with respect to the observer.

Initially we intended to use simplifying assumptions about the distances and the orbits, coupled with the large size of the sample to see if we see any general trends. In the next section this method of classifying the SSOs will be explained. In the end it will turn out that the lack of knowledge about the radial velocity does introduce a large uncertainty into this method.

In section 3.3 I will describe a method of classifying the SSOs based on the paper Milani, Gronchi, et al. 2004, also mentioned section 1.6.2. It turns out that the nature of their admissible region determination allows us to determine an absolute maximum admissible distance for each SSO, without any of the extensive computing necessary for their full determination of the admissible region and best estimate of the orbit. This avoids the pitfalls of the first method, namely the great uncertainty that remains, but it will turn out that this method is highly conservative.

3.2 · Assuming circular orbits

From Mahlke, Bouy, et al. 2018 we know that of the associated SSOs the fast majority are Main Belt Asteroids (MBAs), and while we cannot be completely certain, it is reasonable to extend this assumption to the rest of the harvest. We know that MBAs follow roughly circular orbits, in addition to the Trojan asteroids, and we therefore want to see what happens if we assume the entire sample to have circular orbits. Assuming a perfectly circular orbit simplifies our orbital determination incredibly, heliocentric distances and orbital speeds are then very directly correlated.

The following methodology is implemented within a PYTHON notebook environment.¹

We still do not know any distance of course, geocentric or heliocentric, but by assuming any heliocentric distance (say 3 AU, a reasonable distance for MBAs) we can convert our geocentric coordinates to heliocentric coordinates.

The positions of the SSOs that are retrieved from KiDS using the pipeline are given in geocentric equatorial coordinates. The first step, to simplify and make our calculations more intuitive is to convert our SSO coordinates to the ecliptic system, for this we

¹To be found at: https://gitlab.astro-wisconsin.org/SolarSystem/SSOs_in_KiDS

use equations from the book *Fundamental astronomy* (Karttunen et al. 1987), see also section 1.5.

The equations are as follows, where ϵ is the obliquity of the ecliptic or the angle of the Earth equator with the ecliptic plane (roughly $23^\circ 26'$):

$$\sin \beta = \sin \delta \cos \epsilon - \cos \delta \sin \epsilon \sin \alpha \quad (3.1a)$$

$$\sin \lambda \cos \beta = \sin \delta \sin \epsilon + \cos \epsilon \sin \alpha \quad (3.1b)$$

$$\cos \lambda \cos \beta = \cos \delta \cos \alpha \quad (3.1c)$$

Note that both equations 3.1b and 3.1c are necessary to be able to determine the right quadrant for each new ecliptic longitude, using the signs of the sine and cosine terms.

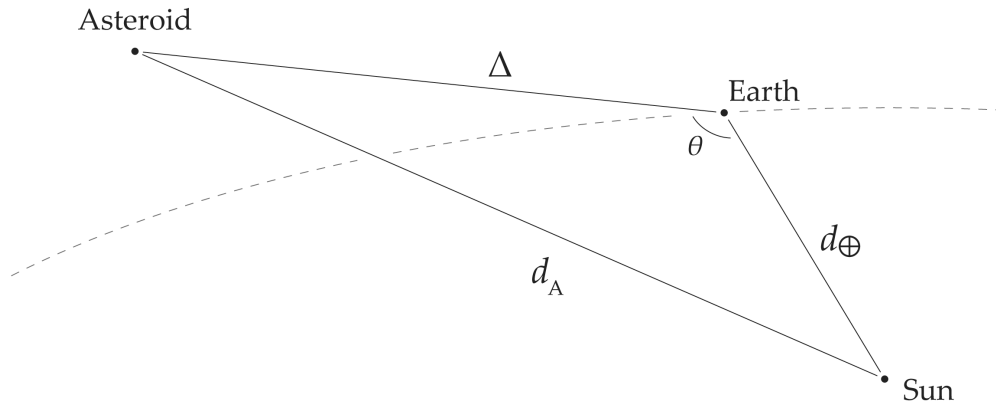


Figure 3.1: A schematic representation of the relevant quantities and positioning of astronomical bodies, used in the formulae to position any asteroid observed in KiDS at a certain distance, d_A from the Sun. Known quantities are the position of the Earth with respect to the Sun (d_\oplus) and the great circle angle (θ) between this d_\oplus and the position of the asteroid with respect to the Earth (Δ). The length of Δ is unknown and has to be calculated.

With our SSO coordinates in ecliptic coordinates, we can look further into the situation at hand, see Figure 3.1, for a schematic representation with the relevant quantities. The position of the Sun at any observational time can be retrieved using an existing routine, in our case we use the `ASTROPY` package (Price-Whelan et al. 2018), and we know the observational coordinates for our SSO, except for the distance.

This means we can determine the angle (θ) between the Earth-SSO observational unit vector ($\hat{\Delta}$) and the Earth-Sun unit vector (\hat{d}_\oplus), both with Earth as their origin. This is done using the modified definition of the scalar product:

$$\cos \theta = \frac{\hat{\Delta} \cdot \hat{d}_\oplus}{\|\hat{\Delta}\| \|\hat{d}_\oplus\|} = \hat{\Delta} \cdot \hat{d}_\oplus \quad (3.2)$$

The angle θ is always between 0 and 180 degrees, with 180 degrees meaning exact opposition of the SSO with respect to the Sun.

Now to determine the distance between the asteroid and Earth (Δ), we can construct the following expression using the law of cosines, within the triangle formed by the asteroid, Sun and Earth:

$$d_A^2 = \Delta^2 + d_\oplus^2 - 2\Delta d_\oplus \cos \theta \quad (3.3)$$

Which we can rewrite as a quadratic equation of Δ , as such:

$$\Delta^2 - 2d_{\oplus} \cos \theta \Delta + d_{\oplus}^2 - d_A^2 = 0 \quad (3.4)$$

Solving this quadratic equation yields one real positive solution for the distance between the Earth and the SSO (the other solution being negative).

By converting both the Sun-Earth vector and the SSO-Earth observational vector into Cartesian coordinates using the newly found distance, we can add both and retrieve the heliocentric position of the asteroid at its observational time.

Now that we have a way of converting geocentric SSO coordinates to heliocentric coordinates for any given heliocentric distance of the asteroid, we can attempt to further convert our apparent motions to heliocentric circular velocities. Note that we do have to disregard any radial velocity component in this analysis as it is unknown, thus we assume that the only movement we see is due to the perpendicular apparent motion we can observe. Technically, this would mean our circular orbit assumption only holds when the SSO is at exact opposition with the Sun, something which is reflected in the results in the next section. For now we disregard this effect.

To obtain the heliocentric proper motion we use a simplified method, based on the fact that the SSO arcs are not just in general very linear, but also selected for linearity by the detection pipeline. So we avoid laborious vector calculations for this tentative method, by simply taking the first and last coordinate of any SSO observation, converting those from geocentric to heliocentric ecliptic coordinates, and subsequently using those to calculate our heliocentric proper motion. Note the definition of celestial proper motion (μ) (Karttunen et al. 1987):

$$\mu_{\lambda} = \Delta\lambda / \Delta t \quad (3.5)$$

$$\mu_{\beta} = \Delta\beta / \Delta t \quad (3.6)$$

$$\mu = \sqrt{\mu_{\beta}^2 + \mu_{\lambda} \cos \beta} \quad (3.7)$$

Where λ and β are their respective celestial coordinates as explained in section 1.5 (and Δ denotes the difference between the first and last observational coordinates), Δt represents the total observation time. The $\cos \beta$ -term is necessary to account for the 'compression' of the longitudes at higher latitudes.

Since we made a prior assumption about the heliocentric distance (d_A), with this distance, we also have the necessary parameters to convert the heliocentric proper motion to a velocity, which we will call v_A . Again, this disregards any radial component to the velocity, but it does ensure the motion is perpendicular to the orbit.

The final step this analysis is to look for the intersect of this supposed circular velocity, v_A , with the true circular orbital velocity that follows from orbital mechanics. Note the simple relation between the circular orbital velocity (v_c) and the radial distance from the body orbited (r): $v_c = \sqrt{\frac{GM}{r}}$, where $GM = \mu$, the standard gravitational parameter. When we vary the assumed distance d_A , getting a different v_A each time, the distance where v_A and v_c match we consider the best estimate for the circular orbital distance for the respective SSO.

Finding this intersect is done with a pre-existing NUMPY routine implementing the Newton-Rhapson Method for root finding. In the end we get a radial distance that

roughly corresponds where the SSO should orbit if it was in a perfectly circular orbit, a distance we will call d_c .

3.2.1 — Results

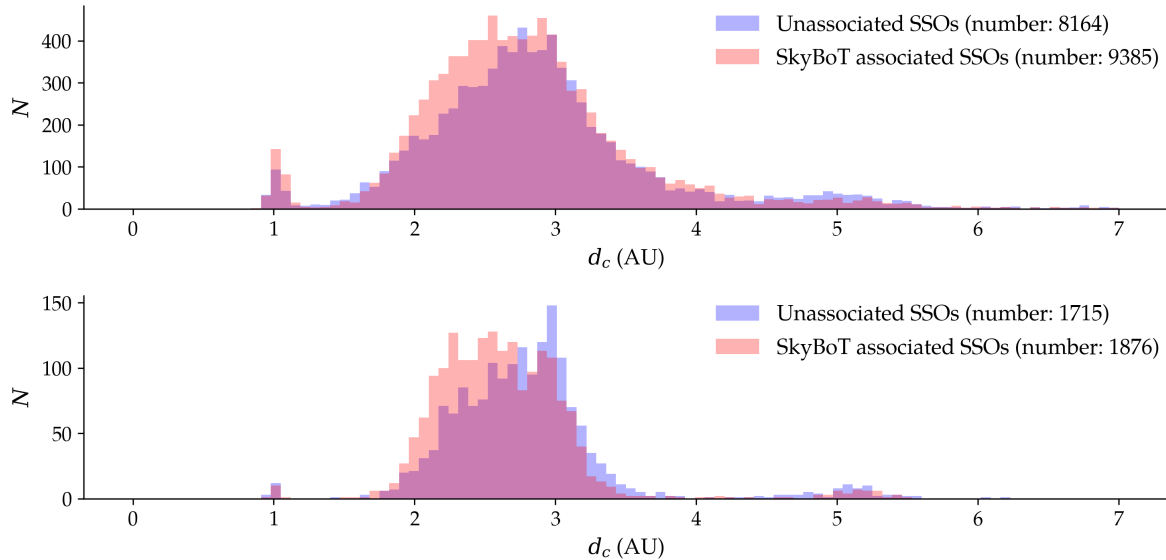


Figure 3.2: The above histograms show the distributions of estimated circular orbital distances (d_c) for the 2018 harvest sample of SSOs distinguishing between SkyBoT associated and unassociated SSOs, firstly without any observing angle constraint (above) and for a sample where the observing angle is restricted to be greater than 170° with respect to the Sun (below). Note that the number of SSOs is indicated for each of the samples.

The results of the circular orbital method analysis when performed on our SSO candidates are shown in 3.2. There exists a remarkable clustering between 2 and 3 AU, even when the current implementation of the method is quite rough. This matches quite neatly with our assumption that most of the SSOs observed are MBAs. It can also be seen that for the SSOs that have not been associated by SkyBoT the distribution is offset slightly to higher distances, consistent with their higher magnitude and therefore presumably farther distance from Earth. Note that for some SSOs the root finding algorithm broke down and no distance was found.

As a caveat, throughout this analysis we have not taken into account radial velocity. This means that a potentially large component of the velocity is disregarded, even if we assume all the SSOs to have perfectly circular orbits. As in the circular case they will still have a radial component when observed from the Earth anywhere except when they are at exact opposition to the Sun. In Figure 3.2 it is shown that this problem can be somewhat avoided by limiting the observing angle (θ), leading to a much sharper distribution. Naturally this also limits the sample we can treat.

To visually inspect the accuracy of the method, Figure 3.3 was created using SSOs with known orbital parameters. Firstly it can be seen that without any constraint on θ the distribution of d_c for the two major population, the MBA and Jupiter Trojans, both with largely circular orbits, is quite spread out. Also some patterns can be observed

around 1 AU, which could be computational peculiarities.

The most striking results is when these two populations are plotted with a constraint on θ ($\theta > 160^\circ$), the correlation between the semi-major axes and d_c is very clear at this point. This begs the question how the distribution would look for all minor planet populations, still with the constraint. As of course for the sample of unknown SSOs we can not select for the populations. We see that even in that case the spread is lesser, however much more present.

It is outside of the scope of this project to find out where the limits of this method lie. Currently it is a proof-of-concept, where the figures are meant to show its potential.

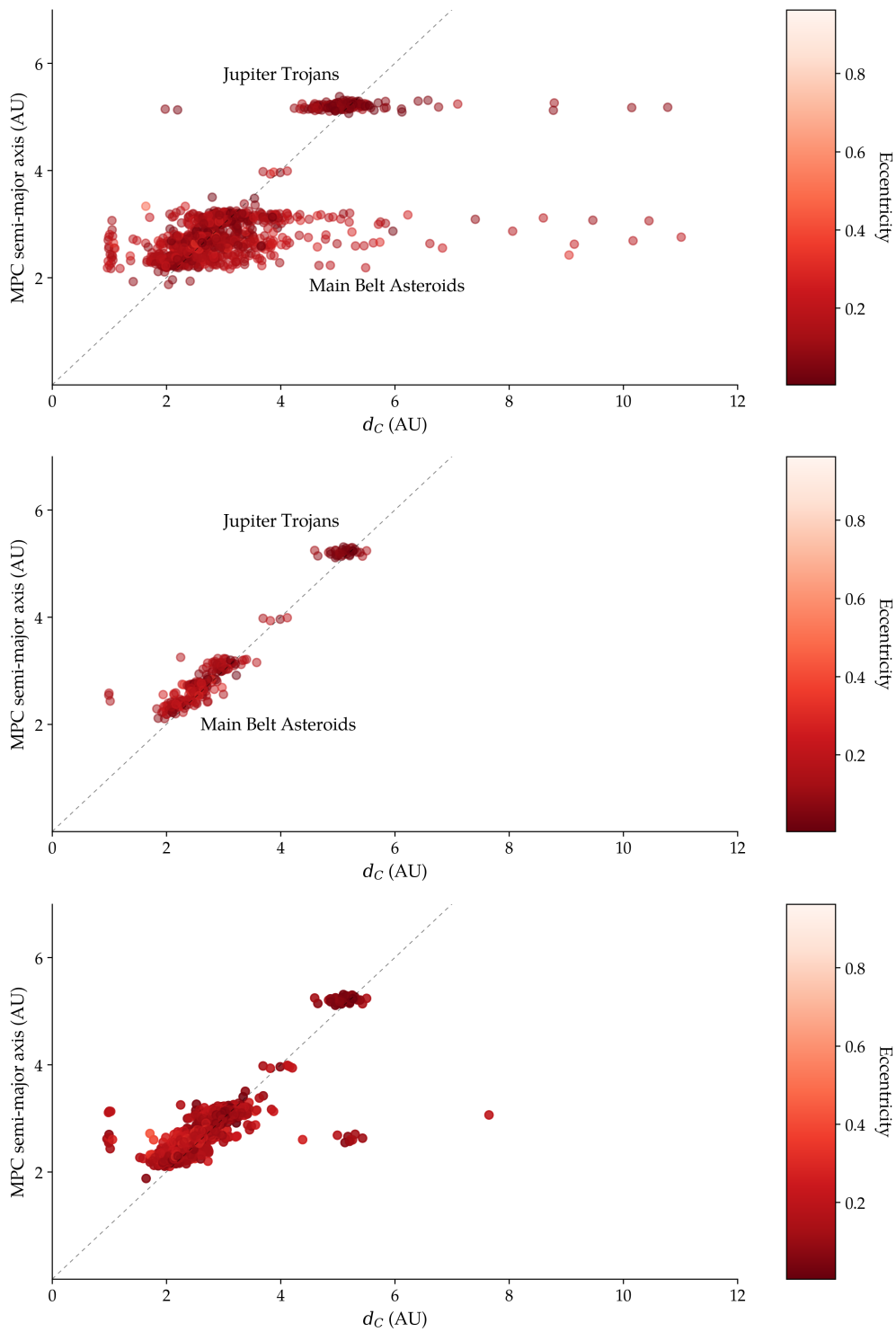


Figure 3.3: The above plots show both the semi-major axes obtained from the Minor Planet Center and the estimated circular orbital velocity (d_c) for associated SSOs with the eccentricities additionally indicated using a colour map. The **top** plot shows the MBA and Trojan minor planet populations with no constraint on the observing angle. The **middle** shows the same populations with an observing angle constrained to be greater than 160° with respect to the Sun. The **bottom** plot shows the SSOs with the same observing angle constraint yet irrespective of minor planet population.

3.3 · Admissable distances

3.3.1 — Method

For this method of classifying the SSOs we build on a version of a method shown in Milani, Gronchi, et al. 2004. In this paper they define an admissible region for any observed SSO based on a set of simple assumptions.

1. The SSO is not a satellite of Earth
2. The SSO's orbit is not determined by the Earth
3. The SSO is bound to the Solar System
4. The SSO is outside of the Earth's surface

Following these assumptions, which are very reasonable for any observed SSO, they build a rigorous mathematical framework for calculating the allowed orbits, primarily based on the gravitational binding energy. For any of the explicit details I will refer the reader to the paper itself.

Relevant for this project are the equations they formed relating the Solar System binding energy (\mathcal{E}_\odot) to the geocentric distance (r) and radial velocity (\dot{r}) at the moment of observation, with constants based on the observational parameters:

$$2\mathcal{E}_\odot(r, \dot{r}) = \dot{r}^2 + c_1\dot{r} + W(r) = \frac{2k^2}{\sqrt{S(r)}} \leq 0 \quad (3.8)$$

Where:

$$W(r) = c_2r^2 + c_1r + c_4 \quad (3.9)$$

$$S(r) = r^2 + c_5r + c_0 \quad (3.10)$$

The exact definitions of the constants (c_i) are given in appendix A.

As equation 3.8 describes the region in which the asteroid is still bound to the Solar System, equating it gives the boundary of this region, beyond which the SSO would be interstellar. We know neither the geocentric distance and radial velocity, however we can infer that the maximum admissible distance is when the radial velocity is zero.

In the case of $\dot{r} = 0$, equation 3.8 reduces to:

$$W(r) - \frac{2k^2}{\sqrt{S(r)}} = 0 \quad (3.11)$$

Which is a sixth order polynomial of r . Of the six roots generally only one is real and non-negative, or occasionally three, in which case the largest distance is taken as our maximum admissible distance.

This formulation is implemented as a python script,² and applied to the SSO candidates. The python script only requires the average observed coordinates and the proper motion detected for each SSO.

This results in maximum geocentric admissible distance for each of the SSO candidates. Following a method explained in section 3.2, these distances can be converted to heliocentric distances, as they, coupled with their celestial coordinates, constitute fully determined geocentric positional coordinates.

²To be found at: https://gitlab.astro-wise.org/SolarSystem/SSOs_in_KiDS

3.3.2 — Results

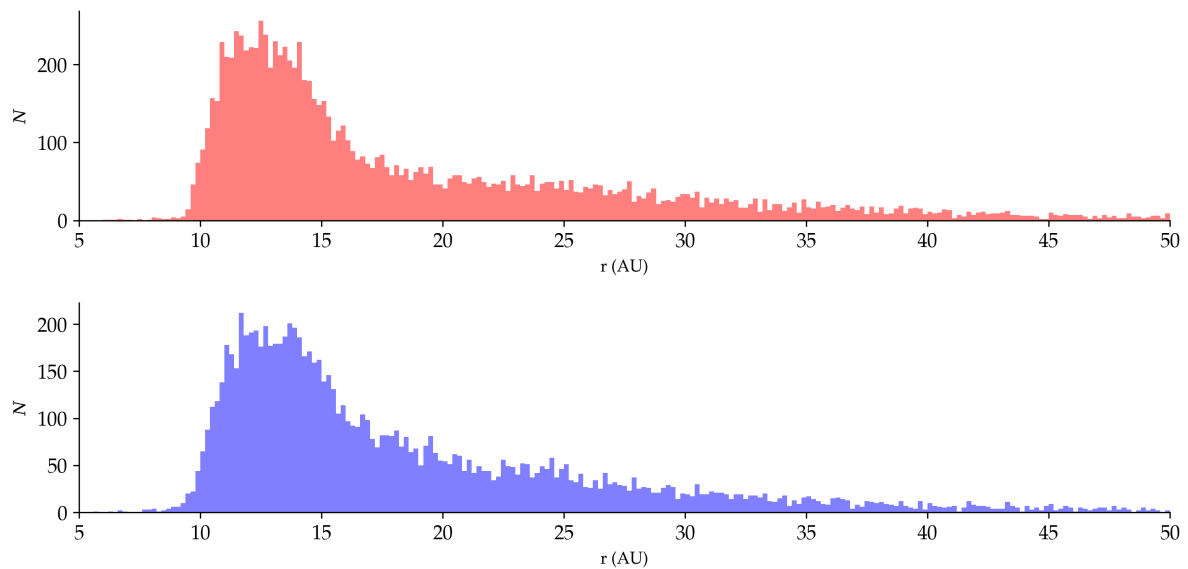


Figure 3.4: The above histograms show the distributions of maximum admissible heliocentric distances, as determined by a method adapted from Milani, Gronchi, et al. 2004 for SSOs detected in KiDS, distinguishing between SkyBoT associated (red, above) and SkyBoT unassociated (blue, below) SSOs. Note that the distributions continue beyond 50 AU, but there are no peaks differing from the general distributions. Also noteworthy is that both the associated and unassociated distributions show little difference.

The overall distributions of the maximum admissible heliocentric distances for the SSO candidates is shown in Figure 3.4. You can see they peak at roughly 14 AU, and show little difference between the SkyBoT associated and unassociated SSOs. Keep in mind that the maximum admissible distance is at the moment of detection, any SSO with – for instance – a highly eccentric orbit could have very different orbital characteristics from any other SSO but get the same maximum admissible distance from our method.

To gain more insight into these results we can look at how they relate specifically to our SkyBoT associated SSOs, as we can get distances for them based on observationally obtained orbital parameters. See Figure 3.5 for a sample of known minor planets that were observed and for whom the maximum admissible distance was calculated. Noticeable is how comparatively conservative the maximum admissible distance is, with respect to the true heliocentric distance.

A few anomalous SSOs (classed as Kuiper Belt Objects), also shown in Figure 3.5, were noticed in the process of developing this method. Namely 2002 CT₁₅₄ which has a much lower determined heliocentric admissible distance to where it truly was, and also exhibited a much higher apparent motion than is typical of KBOs. The implications of this detection will be discussed in the Discussions chapter. Minor planet 2010 JH₁₂₄ is a KBO with a very high eccentricity and is listed as an Unusual Object by the Minor Planet Center.

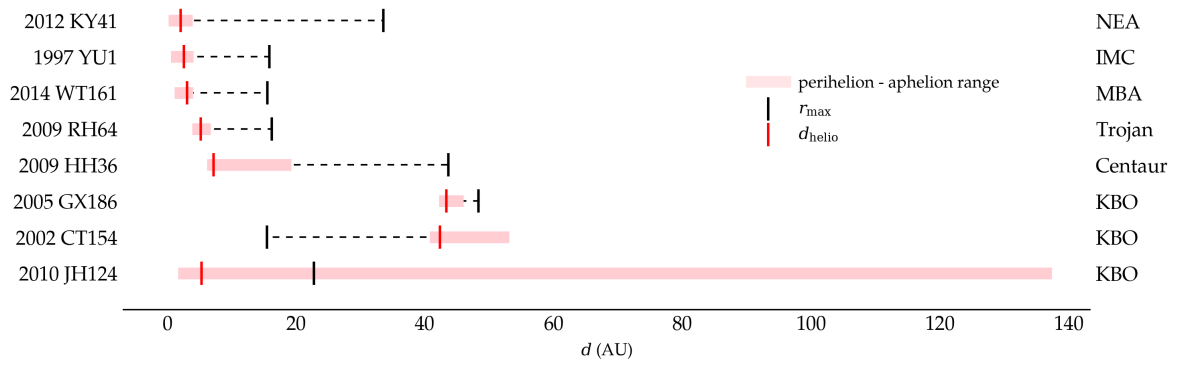


Figure 3.5: The above plot shows how the maximum admissible distances (r_{max}) for a sample of minor planets relate to the true heliocentric distances at the time of observation (d_{helio}) and their peri- and aphelia as obtained from the SkyBoT (Berthier et al. 2006) and Minor Planet Center web services. The SSOs were selected to (randomly) represent a great deal of the minor planets populations (listed on the left for each minor planet, see section 1.4 for the abbreviations), in addition to a few outliers (2002 CT₁₅₄ and 2010 JH₁₂₄).

Discussion

In this chapter the various aspects of this project will be briefly discussed and put into context of current and future research.

4.1 · Serendipitous SSO detection

Looking at the SSO detection pipeline used in this project itself, an analysis of the strengths and weaknesses of the pipeline is already performed in Mahlke, Bouy, et al. 2018. It is outside the scope of this project to treat this further. However, I do wish to refer to the later article on the pipeline, Mahlke, Solano, et al. 2019, which features a much more rigorous description of how the false-positive ratio is obtained.

When considering the wider context of serendipitous SSO detection, it is naturally hard to say what the future will hold. The number of surveys the pipeline could be applied to is potentially very large. In Astro-WISE alone, a number of other VLT surveys could be subjected to the pipeline, such as the VST ATLAS and VPHAS+ surveys, as well as the VIKING survey, an infrared complement to KiDS using VISTA telescope (Arnaboldi et al. 2007). Additionally, one of the drivers behind M. Mahlke's research was the future potential of the Euclid space mission for SSO detection, which is also explored in Carry 2018.

We can only speculate on the potential and statistical significance of serendipitous SSO detection when even larger sets of candidates are available.

4.2 · The circular orbit method

The circular orbital method was meant to extend the detection pipeline with a method to constrain heliocentric distances. While naturally more rigorous methods of orbital distance approximation exist, even for Too Short Arc SSOs, they are generally very computationally intensive, more suited for small samples of observations. The current method is not computationally intensive and can be performed on large numbers of SSO candidates, but holds best for SSO candidates observed near opposition to the Sun ($\theta > 160^\circ$), roughly 20% of the total harvest.

The current implementation is most definitely a proof-of-concept, and has to be treated as such. It is quite rough and its accuracy has not been rigorously tested. Additionally the computational methods may still be improved, as there are still a number of unexplained results. The gathering of SSOs with roots exactly at 1 AU are likely method inherent artefacts, as it should not be possible to determine an estimate of the circular orbital velocity at this distance. When looking at the SSOs that were observed away from Solar opposition we see a spread of roots found beyond 5 AU, a region where we hardly expect any of our observed SSOs to be. Finally, the method does not work for all SSO candidates, it fails for roughly 10% of the sample.

However, the method even in its current form shows remarkably good results overall, with respect to the aim of the method. Future development we hope can lead to a robust system for estimating the orbital distances of large groups of SSO candidates.

The estimation might only improve with larger data sets, especially once one considers the associated SSOs as a prior – in a Bayesian framework – for the method when applied to unassociated SSOs.

Extending the method to, for instance, also include (small) eccentricities could be explored. The problem with introducing any number of additional orbital elements to be studied is that they immediately necessitate additional parameters to be introduced. Introducing eccentricity would for instance require both an argument of periapsis and a longitude of the ascending node to be taken into account. In any case, successfully introducing any number of additional orbital parameters could increase the accuracy of the method tremendously, so it is definitely worthwhile to consider.

As a final remark, quantifying the error induced by observing further away from Solar opposition (so with increasing θ) could strengthen the method.

4.2.1 — Population constraints

As mentioned in section 1.4, minor planet populations are dependent on orbital parameters. Meaning that we can use our estimated heliocentric distances (analogous to semi-major axes) to briefly discuss whether we observe any notable difference between the populations of the SkyBoT associated and unassociated SSOs.

Generally when looking at Figures 3.2 and 3.4, we notice no significant extension in the orbital distances of the unassociated SSOs beyond what can be expected based on the associated ones. We see the distribution of the unassociated asteroids is limited to the usual range of the Main Asteroid Belt (roughly between 2 and 4 AU), however it peaks at a slightly higher heliocentric distance. We can speculate this to mean that we are seeing a greater number of more distant, smaller asteroids in the Main Asteroid Belt, but not a significantly greater number of more distant populations such as the Jupiter Trojans or Kuiper Belt Objects.

4.3 · Maximum admissible distances

The maximum admissible distance method as described in section 3.3 adds a form of foundation to any SSO detection, as a maximum distance is more informative than a comparatively near infinite maximum. Again, simplifying the method from Milani, Gronchi, et al. 2004 hopefully decreases the threshold to usage in any serendipitous SSO detection pipeline.

In the future it might be explored how much of the original method from Milani, Gronchi, et al. 2004 can be re-introduced to extend the current method, without slowing down the algorithm too much. Note however that, for instance, re-introducing the radial velocity component ($\dot{r} \neq 0$) to the formulation would necessitate finding the roots to a function of two parameters. This is significantly more complex.

Additionally the method could be extended by calculating photometric maximum sizes for the SSOs at their maximum admissible distance. This was already partially explored in this project but not included due to time constraints. Both the maximum photometric size and admissible distance could then be used to select samples within any SSO harvest for further study. This is however slightly hampered by the fact that

the maximum admissible distance is known only at the moment of observation, and can therefore not be conclusively used on its own to identify distinct minor planet populations in the sample.

As is also shown in Figure 3.5, at least one associated SSO that was noticed during development, 2002 CT₁₅₄, showed a maximum admissible distance that was much lower than what its true location was at the time of observation. We speculate that this is caused by a misidentification by SkyBoT, considering that the error rate of the association algorithm is of course hard to verify. This opens up another use for the maximum admissible distance method, as it could be used to identify certain grievous misidentifications.

Conclusion

During the course of this Bachelor research project, the SSO pipeline developed by M. Mahlke was used intensively. However due to computing and time constraints, the number of fields studied in the Kilo-Degree Survey was limited to 29 in total, in 31 filter bands, yielding an additional 452 SSO candidates with 0,05% false-positive rate. While not as extensive as intended this harvest proved very useful for getting insight into the workings of the pipeline. In the case of KiDS, further automation within the data processing framework of Astro-WISE can extend the fields searched, and coupled with its future development, the SSO detection pipeline is expected to give many more results both within and outside of KiDS.

The circular orbit method which allows for the estimation of orbital distances for detected SSOs, can provide insight into a large number of the SSOs detected. In particular those SSOs that are considered part of certain major minor planet populations, such as the Main Belt Asteroids and Jupiter Trojans. Yet this method still has to be further verified and detailed.

The method developed to determine maximum admissible heliocentric distances for the detected SSO, has potential for sample selection from the SSO harvests, in addition to possible verification of minor planet associations. It could be further extended with the photometric visual magnitudes to get maximum sizes for the SSOs, adding to its functionality.

To conclude, while none of goals initially set out by this project were fully reached, significant progress was made. The goal of further extending the serendipitous SSO harvest from KiDS in the fourth data release, was furthered with the project's harvest. Similarly, the goal of obtaining more information from the detected SSOs was also reached, through the development of the tentative methods which show potential through good results.

Bibliography

- Arnaboldi, M. et al. (2007). “ESO Public Surveys with the VST and VISTA”. In: *The Messenger* 127, p. 28.
- Begeman, K. et al. (2013). “The Astro-WISE datacentric information system”. In: *Experimental Astronomy* 35.1-2, pp. 1–23. DOI: 10.1007/s10686-012-9311-4. arXiv: 1208.0447 [astro-ph.IM].
- Berthier, J. et al. (2006). “SkyBoT, a new VO service to identify Solar System objects”. In: *Astronomical Data Analysis Software and Systems XV*. Ed. by C. Gabriel et al. Vol. 351. Astronomical Society of the Pacific Conference Series, pp. 367–+.
- Bertin, E. (2006). “Automatic Astrometric and Photometric Calibration with SCAMP”. In: *Astronomical Data Analysis Software and Systems XV*. Ed. by C. Gabriel et al. Vol. 351. Astronomical Society of the Pacific Conference Series, p. 112.
- Bertin, E. and S. Arnouts (1996). “SExtractor: Software for source extraction.” In: *Astronomy and Astrophysics Supplement Series* 117, pp. 393–404. DOI: 10.1051/aas:1996164.
- Capaccioli, M., D. Mancini, and G. Sedmak (2003). “VST: The VLT Survey Telescope”. In: 74, p. 450.
- Capaccioli, M. and P. Schipani (2011). “The VLT Survey Telescope Opens to the Sky: History of a Commissioning”. In: *The Messenger* 146, pp. 2–7.
- Carry, B. (2018). “Solar system science with ESA Euclid”. In: 609, A113, A113. DOI: 10.1051/0004-6361/201730386. arXiv: 1711.01342 [astro-ph.EP].
- de Jong, J. T. A. et al. (2013). “The Kilo-Degree Survey”. In: *The Messenger* 154, pp. 44–46.
- de Jong, Jelte T. A. et al. (2015). “The first and second data releases of the Kilo-Degree Survey”. In: 582, A62, A62. DOI: 10.1051/0004-6361/201526601. arXiv: 1507.00742 [astro-ph.CO].
- Gronchi, Giovanni F. (2005). “Classical and modern orbit determination for asteroids”. In: *IAU Colloq. 196: Transits of Venus: New Views of the Solar System and Galaxy*. Ed. by D. W. Kurtz, pp. 293–303. DOI: 10.1017/S174392130500147X.
- Jedicke, R. et al. (2015). “Surveys, Astrometric Follow-Up, and Population Statistics”. In: *Asteroids IV, Patrick Michel, Francesca E. DeMeo, and William F. Bottke (eds.), University of Arizona Press, Tucson, 895 pp. ISBN: 978-0-816-53213-1, 2015., p.795-813*, pp. 795–813. DOI: 10.2458/azu_uapress_9780816532131-ch040.
- Karttunen, Hannu et al. (1987). *Fundamental Astronomy*. Berlin Heidelberg: Springer-Verlag.
- Kuijken, K. (2011). “OmegaCAM: ESO’s Newest Imager”. In: *The Messenger* 146, pp. 8–11.
- Kuijken, K. et al. (2019). “The fourth data release of the Kilo-Degree Survey: ugrI imaging and nine-band optical-IR photometry over 1000 square degrees”. In: *arXiv e-prints*, arXiv:1902.11265, arXiv:1902.11265. arXiv: 1902.11265 [astro-ph.GA].
- Mahlke, M., H. Bouy, et al. (2018). “Mining the Kilo-Degree Survey for solar system objects”. In: 610, A21, A21. DOI: 10.1051/0004-6361/201730924. arXiv: 1711.02780 [astro-ph.IM].

- Mahlke, M., E. Solano, et al. (2019). "The ssos pipeline: Identification of Solar System objects in astronomical images". In: *Astronomy and Computing* 28, 100289, p. 100289. doi: 10.1016/j.ascom.2019.100289. arXiv: 1906.03673 [astro-ph.EP].
- Milani, Andrea, Giovanni F. Gronchi, et al. (2004). "Orbit determination with very short arcs. I admissible regions". In: *Celestial Mechanics and Dynamical Astronomy* 90.1-2, pp. 57-85.
- Milani, Andrea, Zoran Knežević, et al. (2010). "Dynamics of the Hungaria asteroids". In: *Icarus* 207.2, pp. 769-794. ISSN: 0019-1035. DOI: <https://doi.org/10.1016/j.icarus.2009.12.022>. URL: <http://www.sciencedirect.com/science/article/pii/S0019103509005119>.
- Pater, Imke de and Jack J. Lissauer (2001). *Planetary Sciences*. 2nd ed. Cambridge: Cambridge University Press.
- Price-Whelan, A. M. et al. (2018). "The Astropy Project: Building an Open-science Project and Status of the v2.0 Core Package". In: 156, 123, p. 123. doi: 10.3847/1538-3881/aabc4f.
- Spahr, Timothy B. (2010). *MPEC 2010-U20 : EDITORIAL NOTICE*. <https://www.minorplanetcenter.net/iau/services/MPC.html>. (Accessed on 07/30/2019).
- Spratt, Christopher E. (1990). "The Hungaria group of minor planets". In: 84, pp. 123-131.
- Valentijn, E. A. et al. (2007). "Astro-WISE: Chaining to the Universe". In: *Astronomical Data Analysis Software and Systems XVI*. Ed. by R. A. Shaw, F. Hill, and D. J. Bell. Vol. 376. Astronomical Society of the Pacific Conference Series, p. 491. arXiv: astro-ph/0702189 [astro-ph].

Appendices

A. Constants for equation 3.8

To define the constants necessary for equation 3.8 we need to first define some important quantities.

Firstly, the longitudinal and latitudinal coordinates are given as ϵ and θ respectively, they can both denote ecliptic coordinates (λ and β respectively) or equatorial coordinates (α and δ respectively), for the coordinate systems see section 1.5.

Then, \mathbf{P}_\oplus denotes the heliocentric Earth positional vector, therefore $\dot{\mathbf{P}}_\oplus$ denotes the Earth's heliocentric velocity.

The unit vector $\hat{\mathbf{R}}$ denotes the observation direction of the given SSO. This vector can be extended with unit vectors in the ϵ and θ direction to form an orthogonal basis, as such:

$$\hat{\mathbf{R}}_\epsilon = \frac{\partial \hat{\mathbf{R}}}{\partial \epsilon} = (-\sin \epsilon \cos \theta, \cos \epsilon \cos \theta, 0) \quad (1)$$

$$\hat{\mathbf{R}}_\theta = \frac{\partial \hat{\mathbf{R}}}{\partial \theta} = (-\cos \epsilon \sin \theta, -\sin \epsilon \sin \theta, \cos \theta) \quad (2)$$

Finally, η denotes the proper motion, such that $\eta = \sqrt{\dot{\epsilon}^2 \cos^2 \theta + \dot{\theta}^2}$.

The constants as used in equation 3.8 are then:

$$c_0 = \|\mathbf{P}_\oplus\|^2 \quad (3)$$

$$c_1 = 2\langle \dot{\mathbf{P}}_\oplus, \hat{\mathbf{R}} \rangle \quad (4)$$

$$c_2 = \eta^2 \quad (5)$$

$$c_3 = 2\dot{\epsilon} \langle \dot{\mathbf{P}}_\oplus, \hat{\mathbf{R}}_\epsilon \rangle + 2\dot{\theta} \langle \dot{\mathbf{P}}_\oplus, \hat{\mathbf{R}}_\theta \rangle \quad (6)$$

$$c_4 = \|\dot{\mathbf{P}}_\oplus\|^2 \quad (7)$$

$$c_5 = 2\langle \mathbf{P}_\oplus, \hat{\mathbf{R}} \rangle \quad (8)$$

B. ADASS poster

See following page

Mining the Kilo-Degree Survey for Solar System Objects

yadevries@astro.rug.nl



Software for tentative classification of serendipitously observed asteroids

Supervised by: G.A. Verdoes Kleijn
K. Frantseva

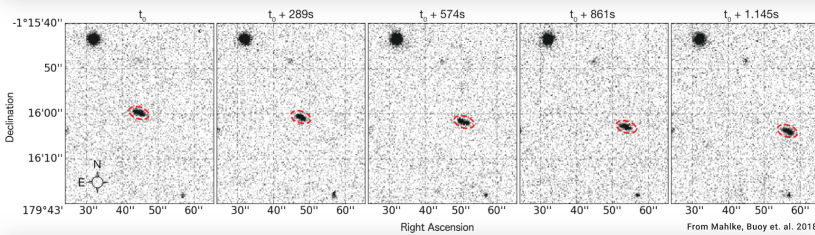
Ylse Anna de Vries

Introduction

This **Bachelor Research Project** aims to detect **Solar System objects (SSOs)** in the **Kilo-Degree Survey (KIDS)** using an existing **SSO detection pipeline**. We explore **constraining distances for these transient detections** by extending the pipeline with software.

KIDS is a wide-field optical imaging survey that uses the OmegaCAM imager of the **VLT Survey Telescope (VST)** at the ESO Paranal observatory in Chile. All KIDS data is calibrated and archived in **Astro-WISE**, an information system that connects an international network of storage servers, computing clusters, and databases.

The **main focus of KIDS** is to study weak gravitational lensing and redshifts to constrain the cosmological matter distribution. However the same observations can also be used to serendipitously discover SSOs.



The SSO detection pipeline

The SSO detection pipeline used in this project was developed by **Max Mahlke** as published in Mahlke, Bouy et al. 2018. [QR](#)

The **principal aim** of the pipeline is detecting the SSOs' apparent celestial motion across the timespan between exposures, see the figure above.

The pipeline first uses **SExtractor** and **SCAMP** on individual KIDS exposures retrieved from Astro-WISE, see the box diagram to the left, to extract moving sources.

Subsequent **filtering to exclude contaminants** (such as cosmic rays, diffraction patterns, bright star halos) is performed using a **python script**.

The pipeline uses **web-based services** extensively, such as the **IMCCE SkyBoT service**, which associates known minor planets with the SSO detections.

The pipeline was performed on **362 square degrees** of KIDS. Resulting in **20673 SSO candidates** with a 0,05% false-positive rate.

Discussion and conclusion

The SSO detection pipeline was successfully run on an additional **31 square degrees** for this project, more could not be studied due to time and computing constraints.

In the future the pipeline could be automated and run on all KIDS fields, and potentially the other surveys in Astro-WISE.

The **circular orbit method** of analysing the detected SSOs shows potential, but has to be expanded and validated to be useful. It is now a **proof-of-concept**.

The **admissible regions approach** could be used as **validation** for existing detections and minor planet associations, and for **selecting samples** for future study from any serendipitous SSO detections.

With the potentially **large number of yet undiscovered SSO candidates** in existing and future surveys the pipeline could open up a **large set of new data**. See Mahlke, Solano et al. 2019 [QR](#) for further development of the pipeline.

THE DATA FLOW

KIDS VST DATA



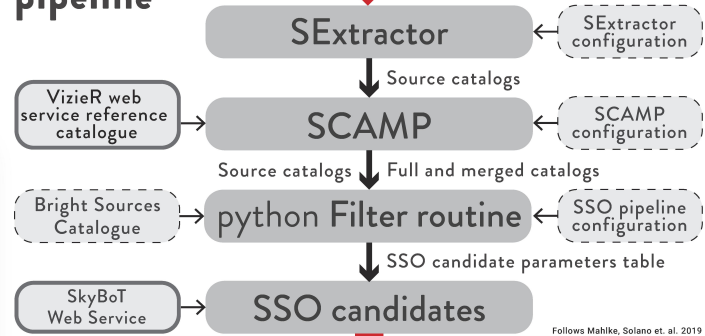
Astro-WISE

KIDS data gets photometrically and astrometrically calibrated using the calibration pipeline in Astro-WISE.

For one square degree KIDS tile the SSO detection pipeline analyzes per filter up to 5 dithers x 32 detectors = 160 calibrated detector frames of 2000x4000 pixels.

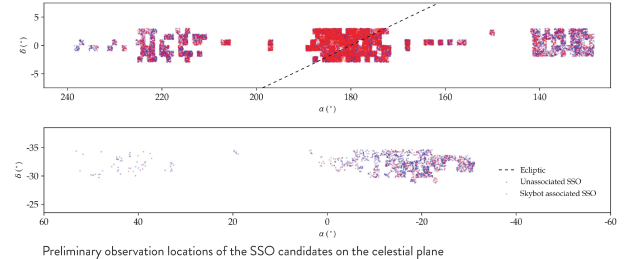
RegriddedScienceFrames

The SSO detection pipeline



Follows Mahlke, Solano et al. 2019

SSO candidate observation locations

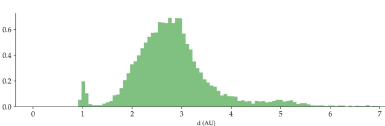


Link to full BSc thesis (includes references)



Circular orbit method

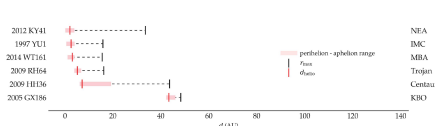
Using the assumption that many SSOs will be minor planets with **roughly circular orbits**, we use this assumption to get **estimates of the semi-major axes** for the entire sample of SSO candidates.



Preliminary distribution of the estimated semi-major axes of the SSO candidates, using the method mentioned above.

Admissible regions method

Using a method from Milani, Gronchi, et al. 2004 [QR](#), we calculate a **maximum admissible distance** for each SSO candidate. This allows for a (conservative) upper limit to the heliocentric distance and size of the SSO.



Maximum heliocentric admissible distance compared to the true heliocentric distance for a number of known SSOs.

